Proceedings of the Thirty-third (2023) International Ocean and Polar Engineering Conference **www.isope.org**
Ottawa, Canada, June 19-23, 2023

ISBN 978-1-880653-80-7; ISSN 1098-6189

Numerical Simulation of Sloshing Flows of Three-Dimensional Rectangular Tank in Regular Waves by MPS Method

*Congyi Huang[1], Jifei Wang[2], Decheng Wan[1]**

[1] Computational Marine Hydrodynamic Lab (CMHL), School of Naval Architecture, Ocean and Civil Engineering, Shanghai Jiao Tong University, Shanghai, China
[2] Shanghai Aerospace System Engineering Institute, Shanghai, China
*Corresponding author

ABSTRACT

During the navigation of a LNG carrier, the cabin will heave, pitch or have other motions in waves, which will stimulate the liquid sloshing inside the tank. The liquid sloshing inside and the waves outside act on the cabin at the same time, making it have a relatively complex movement. In this paper, meshless particle method is used to simulate the internal and external coupling problem. The motion of the liquid carried cabin and the solid carried cabin in regular waves are simulated by MPS method and compared each other to analyze the influence of the liquid sloshing on the sway motion of the cabin. Next, the influence of filling rate on liquid sloshing is studied, three cases of filling rate of 25%, 50% and 75% are simulated, finding that the liquid sloshing is the most severe when the filling rate is 50%. Whether the liquid sloshing promotes or inhibits the cabin sway motion depends on the phase difference between regular wave and liquid sloshing.

KEY WORDS: Moving Particle Semi-implicit (MPS); regular wave; internal and external flow coupling; sloshing in liquid tank; fluid structure coupling.

INTRODUCTION

Liquid sloshing refers to the fluctuation phenomenon inside a partially loaded cabin under external excitation, whose characters are large free surface deformation and nonlinear wave breaking. With the increasing demand for energy in the world, there are more and more ships used to carry oil and liquefied natural gas (LNG). When these partially loaded liquid cargo ships are sailing at sea, the liquid inside will be sloshing, which will harm the structure strength and the ship operation. Therefore, many researchers have carried out research on the mechanism characteristics of liquid sloshing.

Faltinsen(1987) derived the analytical solution of two-dimensional liquid sloshing under horizontal excitation firstly. Nakayama and Washizu(1980,1981) analyzed the two-dimensional liquid sloshing problem with finite element method (FEM) and boundary element method (BEM) respectively. Xue and Lin (2011) simulated the liquid sloshing phenomenon inside a three-dimensional rectangular tank using the fluid volume method (FVM) and analyzed the inhibition effect of the baffle. Although the mesh-based method has been widely used in simulating the liquid sloshing inside a cabin, it still has some difficulties in dealing with the strong nonlinear problems such as wave breaking, free surface rolling and so on.

MPS (Moving Particle Semi-Implicit) method is a meshless particle method, in which the computational domain is represented by a series of particles without fixed topology relationship. The calculation tracks the movement of the particles, which makes it easy to capture the free surface. So MPS method well suited for simulating problems with the properties of large deformation on free surface, such as wave breaking, splashing and free surface curling. MPS method is also widely used to study the liquid sloshing phenomenon. Rueda et al.(2008) applied MPS to simulate the motion of a fluid chamber in wave, and the amplitude response operator obtained by Fourier transform was consistent with the experimental results. Tsukamoto et al.(2011) arranged a floating body in the middle of a two-dimensional tank, which is connected to the bulkhead by springs. The fluid force on the floating body under different filling rates and excitation frequencies were calculated by MPS method. Zhang et al. (2014) applied the improved MPS method to simulate the two-dimensional liquid sloshing problem. The calculated results are compared with results obtained by the experimental and mesh-based method results, showing that the slamming pressure and the deformation of the free surface are in good agreement. Zhang et al. (2018, 2016) combined MPS with FEM to study the sloshing phenomenon in an elastic liquid tank and the inhibition effect of an elastic baffle. Wen et al. (2018a, 2018b) developed the MPS method for multiphase flow and applied it to the liquid sloshing problem of two and three-layer fluids. The calculated wave height and slamming pressure are in good agreement with the experimental results. Cezar et al. (2019) simulated the sloshing within box-shaped tanks equipped with perforated bulkheads used MPS method. The investigation considered a broad range of parameters, which includes several open-area ratios and different filling levels under pitching excitations encompassing the first three sloshing resonant modes of a non-compartmented tank. Sanchez-Mondragon (2022) et al. combined the Sub-Particle-Scale Large Eddy Simulation (SPS-LES) turbulent model

with the MPS method to identify the turbulent effects due to global motions on a prismatic LNG tank for two filling fractions. Felix-Gonzalez et al. (2022) applied the MPS method to compare the influence of the ship's rotational center location on the exerted forces and moments due to sloshing.

In this paper, the in-house MPS solver MLParticle-SJTU is used to simulate the liquid sloshing inside a cabin moving in regular waves. The slamming pressure inside the cabin and the sway motion of the cabin is recorded. And the influence of the filling rates on the liquid sloshing is analyzed.

NUMERICAL METHOD

The MPS method is a meshless particle method based on the Lagrange representation method. The computational domain is represented by discrete particles. These particles are not connected by grids or nodes, but carry physical quantities such as mass, velocity and acceleration separately. The flow field is controlled by establishing the governing equation.

Governing equations

The governing equations include the continuity equation and the momentum equation. The governing equation for viscous incompressible fluid can be written as:

$$\frac{1}{\rho}\frac{D\rho}{Dt} = -\nabla \cdot \boldsymbol{V} = 0 \tag{1}$$

$$\frac{D\boldsymbol{V}}{Dt} = -\frac{1}{\rho}\nabla P + \nu \nabla^2 \boldsymbol{V} + \boldsymbol{g} \tag{2}$$

where ρ is fluid density, $\boldsymbol{V}$ is velocity vector, P presents pressure, ν is kinematic viscosity, $\boldsymbol{g}$ is gravitational acceleration vector, t indicates time.

Discretization of the governing equations

In the MPS method, the computational domain is composed of discrete particles. Therefore, the governing equations need to be discretized.

Kernel function

In the MPS method, the interaction between particles is realized by the kernel function, which can be written as:

$$W(r) = \begin{cases} \dfrac{r_e}{0.85r + 0.15r_e} - 1 & 0 \le r < r_e \\ 0 & r_e \le r \end{cases} \tag{3}$$

where $r = |\boldsymbol{r}_j - \boldsymbol{r}_i|$ represents the distance between particle i and j, r_e is the influence radius.

Density of the particle number

The particle number density is the sum of kernel functions of all the particles within the influence radius, which can be written as:

$$\langle n \rangle_i = \sum_{j \ne i} W\left(|\boldsymbol{r}_j - \boldsymbol{r}_i|\right) \tag{4}$$

for incompressible fluid, the particle number density remains constant.

Gradient model

The gradient model is used to discretize the pressure gradient in the governing equation. The expression is:

$$\langle \nabla P \rangle_i = \frac{D}{n^0} \sum_{j \ne i} \frac{P_j + P_i}{|\boldsymbol{r}_j - \boldsymbol{r}_i|^2} (\boldsymbol{r}_j - \boldsymbol{r}_i) W(|\boldsymbol{r}_j - \boldsymbol{r}_i|) \tag{5}$$

where D represents the dimension and n^0 represents the initial particle number density.

Divergence model

Similar to the gradient model, the divergence model is used to discretize the velocity divergence in the governing equation. The expression is:

$$\langle \nabla \cdot \boldsymbol{V} \rangle_i = \frac{D}{n^0} \sum_{j \ne i} \frac{(\boldsymbol{V}_j - \boldsymbol{V}_i) \cdot (\boldsymbol{r}_j - \boldsymbol{r}_i)}{|\boldsymbol{r}_j - \boldsymbol{r}_i|^2} W(|\boldsymbol{r}_j - \boldsymbol{r}_i|) \tag{6}$$

Laplacian model

Laplacian model is used to discretize the second derivative in the governing equation, which can be expressed as:

$$\langle \nabla^2 \phi \rangle_i = \frac{2D}{n^0 \lambda} \sum_{j \ne i} (\phi_j - \phi_i) W(|\boldsymbol{r}_j - \boldsymbol{r}_i|) \tag{7}$$

where λ represents the correction of the error introduced by the kernel function, and it can be written as:

$$\lambda = \frac{\sum_{j \ne i} W\left(|\boldsymbol{r}_j - \boldsymbol{r}_i|\right) |\boldsymbol{r}_j - \boldsymbol{r}_i|^2}{\sum_{j \ne i} W\left(|\boldsymbol{r}_j - \boldsymbol{r}_i|\right)} \tag{8}$$

Pressure Poisson equation

In the MPS method, the Poisson equation is used to solve the particle pressure. The incompressibility of fluid is determined by divergence-free condition and constant particle number density condition. The Poisson equation adopted in this paper is as follows:

$$\langle \nabla^2 P^{k+1} \rangle_i = (1-\gamma)\frac{\rho}{\Delta t} \nabla \cdot \boldsymbol{V}_i^* - \gamma \frac{\rho}{\Delta t^2} \frac{< n^k >_i - n^0}{n^0} \tag{9}$$

where superscripts k and k+1 represent k and k+1 time steps. γ is a variable parameter, representing the proportion of particle number density in the source term of Poisson equation. In the numerical simulation in this paper, γ takes 0.01. (Lee et al 2011; Tanaka and Masunaga, 2010)

Detection of free surface particles

When solving the Poisson's pressure equation, it is very important to determine whether a particle is located on a free surface. The number density of particles can be used to determine whether a particle is on a free surface in MPS method. When $\langle n \rangle_i < 0.8 n^0$, the particle is considered to be on a free surface. When $\langle n \rangle_i > 0.97 n^0$, the particles are thought to be inside the fluid. For particles with particle number density between 0.8 and 0.97, it's difficult to tell whether the particle is on the free surface or inside the fluid. Khayyer and Gotoh(2009) first proposed the criterion which simply based on the fact that for a free-surface particle, the distribution of neighboring particles is asymmetric. In this paper, the vector function $\boldsymbol{F}$ presented by Zhang et al (2014) is introduced, as follows:

$$< \boldsymbol{F} >_i = \frac{D}{n^0} \sum_{j \neq i} \frac{(\boldsymbol{r}_i - \boldsymbol{r}_j)}{|\boldsymbol{r}_i - \boldsymbol{r}_j|} W(|\boldsymbol{r}_i - \boldsymbol{r}_j|) \tag{10}$$

If $\langle |\boldsymbol{F}| \rangle_i > 0.9 |\boldsymbol{F}|^0$, the particle i will be considered to be on a free surface. $|\boldsymbol{F}|^0$ stands for $|\boldsymbol{F}|$ at the initial time of the free surface particle.

The accuracy of the MLParticle-SJTU solver has been verified in the published papers. Chen et al. (2019) simulated the sloshing phenomenon of the tank in the LNG tank, and the time-history curve of the pressure measuring point obtained was well coupled with the test results, which verified the accuracy and stability of the solver.

NUMERICAL SIMULATIONS

In this section, the movement of the cabin containing liquid in regular waves is simulated by MPS method, and the effects of the free surface on the slamming pressure and the cabin motion is analyzed.

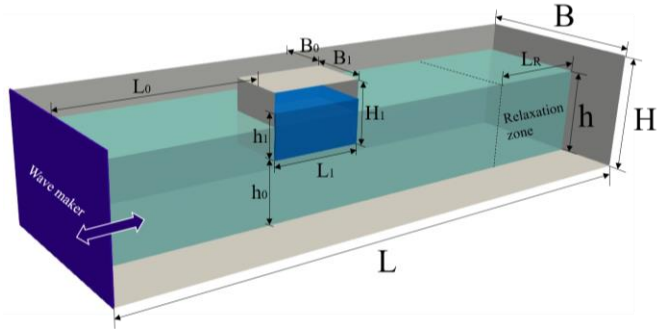

Fig. 1 Schematic diagram of initial calculation model

The initial calculation model is shown as Fig. 1, a rectangular cabin is placed inside a tank. There is a wave making plate on the left side of the tank, and the wave relaxation zone is set on the right side. In this paper, the regular wave is generated by the piston wave making method. Based on linear wave theory, the motion of wave-making plate can be written as:

$$x(t) = \frac{H}{2} \left(\frac{2kh + \sinh(2kh)}{4\sinh^2(kh)} \right) \sin(\omega t) \tag{11}$$

where H represents wave height, h is the water depth and k is wave number. The relaxation zone is placed on the right side of the tank to avoid the wave reflection. The length of the relaxation zone L_R=3m. The artificial viscous term $f_R(x)$ is added to the momentum equation in the relaxation zone, which can be written as:

$$f_R(x) = \begin{cases} -\rho \alpha_R \dfrac{x - x_R}{L_R} \boldsymbol{u} \\ 0 \end{cases} \tag{12}$$

where x_R is the starting position of the relaxation zone, $\boldsymbol{u}$ is fluid velocity, α_R is artificial viscosity coefficient used to control the level of wave relaxation. In this paper, α_R=50.

For the generated regular waves, wavelength is λ=3m and wave height is H=0.3m. The cabin is placed L_0=3m away from the wave maker. The distance between the side wall of the cabin and the tank is B_0=1m, and the bottom of the cabin is h_0=1m away from the tank. The water depth in the tank is h=1.5m, and the water depth inside the cabin is h_1=0.5m in this section. The weight of the cabin is set to 367kg. More details about the dimensions of the calculation model is shown in Table 1. Three pressure measuring points are arranged on the bottom plate of the cabin, with X-direction coordinates x_1=3m, x_2=3.75m, x_3=4.5m separately, as shown in Fig. 2. The distance between two particles is set as Δx=0.04m, the wave length λ=75Δx, with 796998 particles in total. The time step is set as 0.0005s.

Table 1 Dimensions of the calculation model

Symbol	Quantity(m)
L	9.5
B	3
H	2
h	1.5
L_1	1.5
B_1	1
H_1	1
h_1	0.16
L_0	3
B_0	1
h_0	1
L_R	3

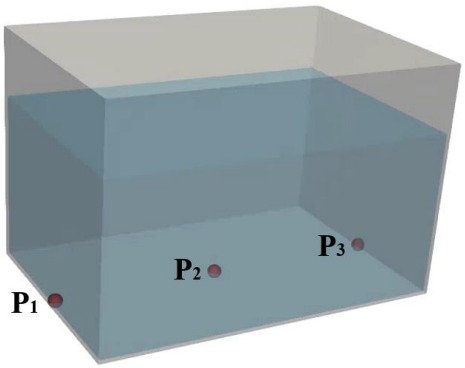

Fig. 2 Schematic diagram of pressure points at the bottom of the cabin

The cabin reciprocates in regular waves. In this paper, only the freedom of the cabin in the X-axis direction is released, and only the sway motion of the cabin is considered. In order to prevent the cabin from drifting along the X-axis in the water tank, the mooring system is arranged on the cabin with a stiffness of 2kN/m. The wavelength of the regular wave is 3m. Based on the dispersion relation of the Airy wave, the period of the regular wave can be calculated to be about 1.4s. Fig. 3 shows the flow field pressure at some moments in the two cycles. As can be seen from the figure, MLParticle-SJTU solver simulates the flow field inside and outside the cabin accurately and appropriately. Outside the cabin, the pressure distribution of the flow field is uniform and stable. The regular wave maintains its shape until it propagates to the cabin. When passing by the cabin, the wave propagation is blocked, and the waves can only pass along the cabin sides or beneath the cabin. Behind the tank, waves transmitted from several directions converge, and the shape of the flow field is rather irregular, which is well simulated by the solver used in this paper. Inside the cabin, the MLParticle-SJTU solver also simulates the flow field pressure and captures the free surface accurately. The internal fluid, stimulated by the movement of the cabin, also reciprocates periodically, slamming the bulkheads on front and back sides of the cabin. There is no surface rolling or breaking phenomenon exists inside the cabin because the liquid motion inside the cabin is not very violent.

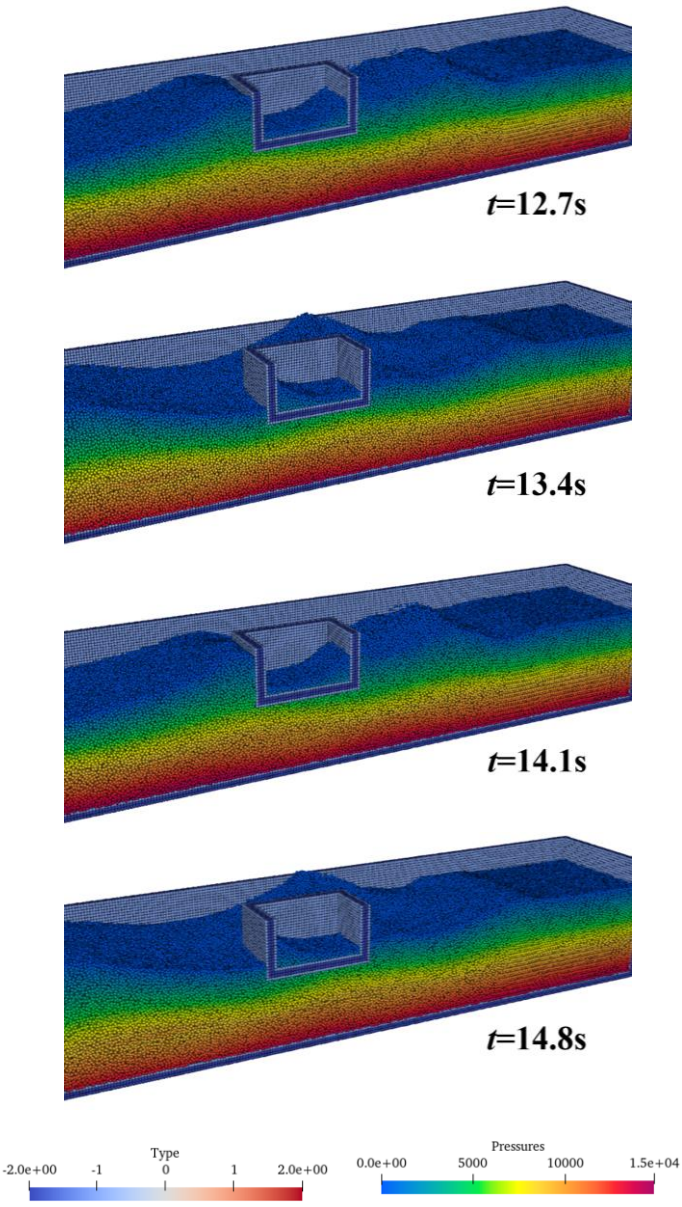

Fig.3 Schematic diagram of flow field pressure for h_1=0.16m

Fig. 4 and Fig. 5 show the pressure time curves of P1 and P3 at the bottom of the tank respectively. The red lines in the figures show the hydrostatic pressure of the cabin at rest. As can be seen from the figures, the time-history curves of the two pressure measuring points show obvious periodic characteristics, and the period is about 1.4s, the same as the regular wave period. There are two peaks of the pressure time curves for each period. By observing the flow field corresponding to the occurrence time of the two peaks respectively, it can be analyzed that the first pressure peak P_{max1} is formed by the fluid slamming the bulkhead, and then the pressure falls slightly. Then the fluid climb upwards along the bulkhead, forming the second pressure peak P_{max2}. For measuring point P1, the first pressure peak is higher than the second one, indicating that the slamming pressure is greater than the water pressure at the maximum depth. For P2, the difference between the first and the second peak is small. The differences between P1 and P3 indicates asymmetry of the simulated sway phenomenon. The forward bulkhead is subjected to higher slamming pressure caused by the liquid sloshing inside the cabin.

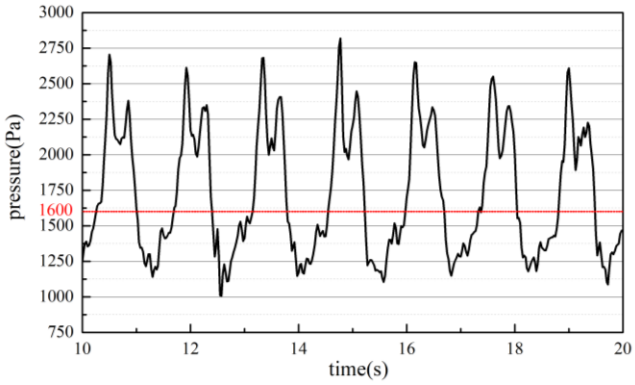

Fig.4 Pressure time curve at measuring point P1 for h_1=0.16m

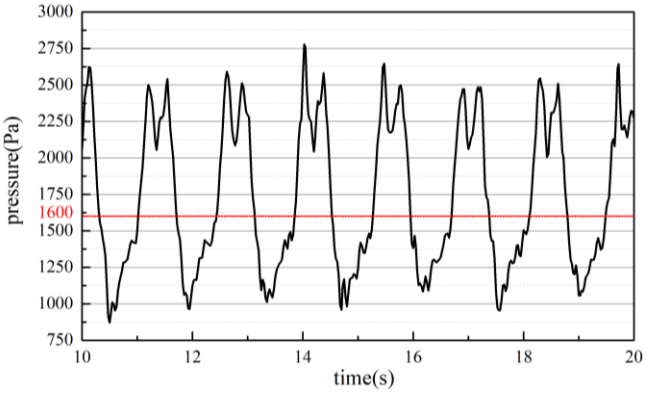

Fig.5 Pressure time curve at measuring point P2 for h_1=0.16m

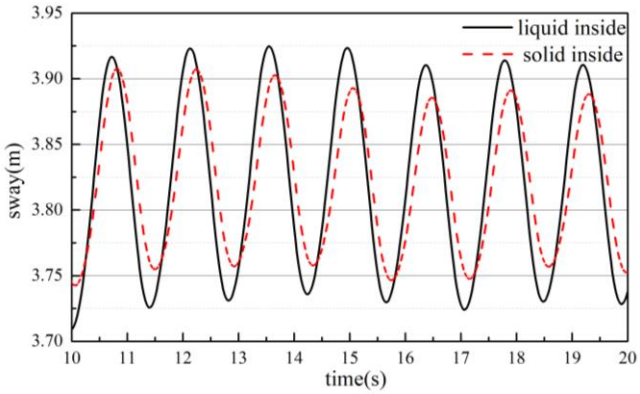

Fig.6 Comparison of sway motion between liquid cabin and solid cabin for h_1=0.16m

The motion of solid tank in the same regular wave is simulated to analyze the influence of liquid sloshing on the motion of cabin. The mass and volume of solid inside the cabin are as same as the liquid inside the cabin mentioned earlier. The X-axis coordinate of the gravity center of the cabin is recorded to present the sway motion. Figure XX shows the comparison of time history curves between liquid tank and solid tank during 10s-20s. As can be seen from the figure that the liquid tank and the solid tank reciprocate in a fixed area, and the period is the same as that of the regular wave, about 1.4s, which conforms to the characteristics of the motion excited by regular waves. The motion amplitude of liquid cabin is larger than that of solid cabin, and the phase of liquid cabin motion is slightly earlier than that of solid cabin,

which indicates that the liquid sloshing inside the cabin promotes the movement of the tank at this filling rate.

Next, the depth of the liquid in the tank is changed and the cabin motion in regular waves is simulated to analyze the influence of the depth of the liquid inside the cabin on the liquid sloshing and the cabin motion. The filling rate is set as 50% and 75%, corresponding to h_1=0.32m and h_1=0.52m inside the cabin respectively. Fig.7 and Fig. 8 show the pressure distribution of the fluid field at two liquid filling rates. As can be seen from Fig.7, when h_1=0.32m, the free surface deformation in the tank is severe with the surface curling and the wave breaking. For such phenomena, the meshless method used in this paper has a unique advantage, which can capture the free surface accurately. For h1=0.52, as can be seen from Fig.8, the top bulkhead of the cabin suppresses the liquid sloshing due to the high filling rate and the fluid accumulated near the bulkhead.

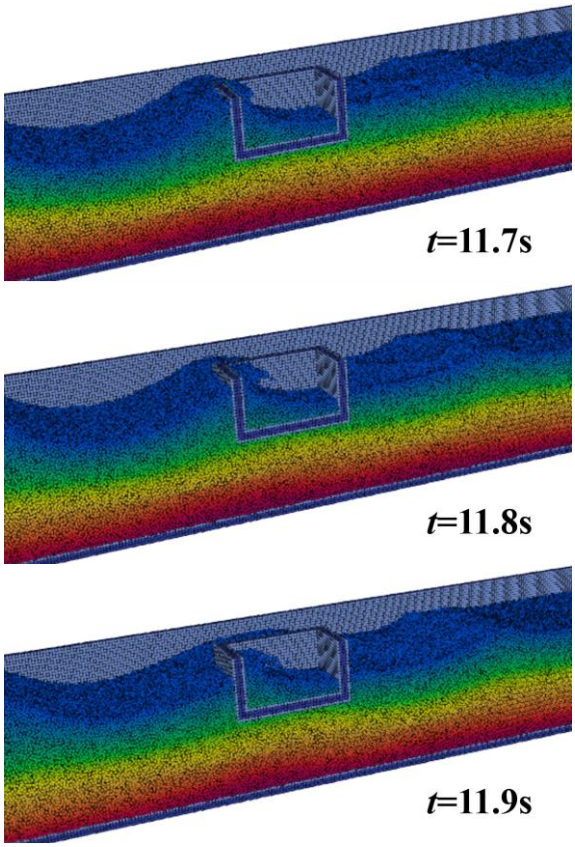

Fig.7 Schematic diagram of flow field pressure for h_1=0.32m

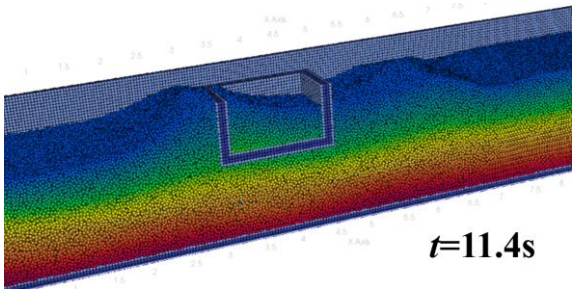

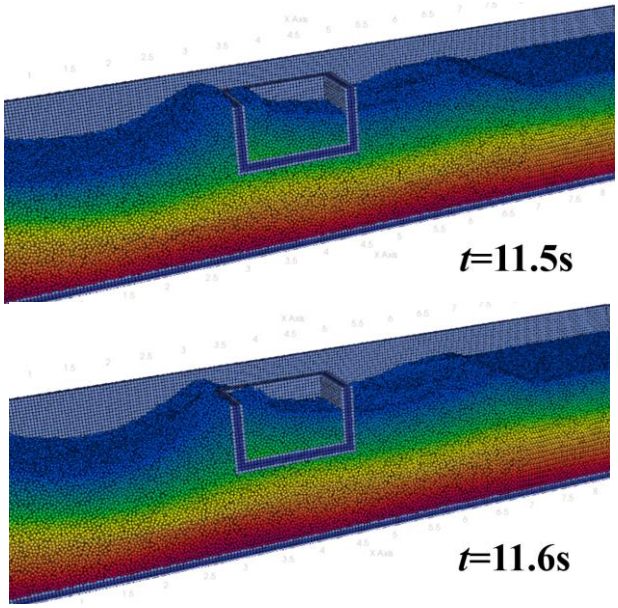

Fig.8 Schematic diagram of flow field pressure for h_1=0.52m

Fig.9 ~Fig.12 show the pressure time curves measured at the two pressure measuring points P1 and P3 under two kinds of liquid filling rates respectively. The red lines represent the hydrostatic pressure at the two filling rates.

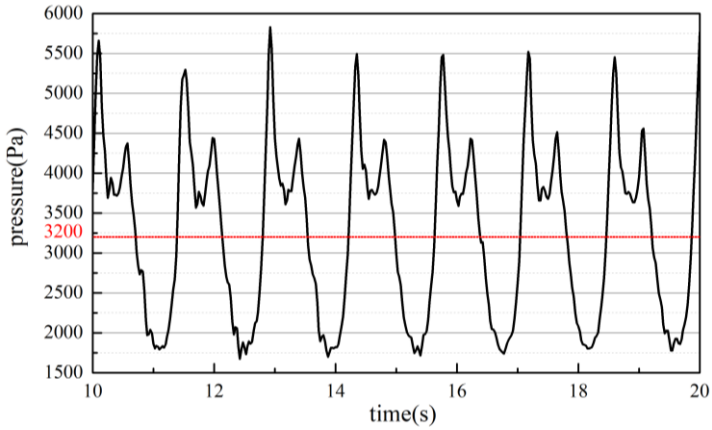

Fig.9 Pressure time curve at measuring point P1 for h_1=0.32m

Consider the part above the red hydrostatic pressure line as the pressure caused by tank swaying. The pressure curve above the hydrostatic pressure line is regarded as the influence of the liquid sloshing. For h_1=0.32m, the pressure time curve characteristics of P1 consistents with that of h_1=0.16m mentioned above. There are two peaks within a period and the first peak is higher than the second one. When h_1=0.32m, the pressure caused by liquid sloshing is about 2300Pa, and when h_1=0.16m, this part of the pressure is about 1000Pa. This shows that the sloshing is more severe and the slamming pressure is greater when the liquid filling rate is 50%. The pressure curve of P3 is relatively similar to that of P1, indicates that the liquid sloshing hits the front and back bulkheads of the tank evenly.

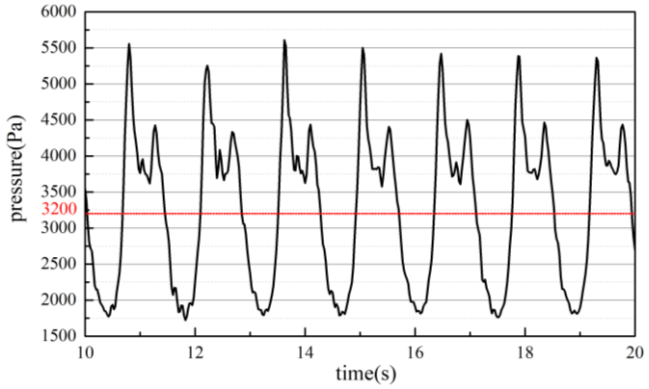

Fig.10 Pressure time curve at measuring point P3 for h_1=0.32m

When h_1=0.52m, the pressure curve of measuring point P1 also presents two peaks in a period. But for P3, there are no two obvious peaks for the pressure curve, but the curve fluctuates around the peak value. This is because the hatch cover prevents the liquid from climbing up along the bulkhead, weakens the energy of the liquid sloshing, and reduces the slamming pressure. The liquid accumulates on one side of the tank, so the the pressure at the measuring point fluctuates around a fixed value because the water depth is the same.

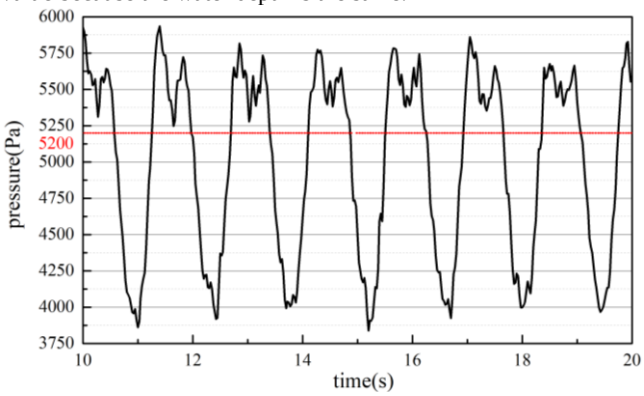

Fig.11 Pressure time curve at measuring point P1 for h_1=0.52m

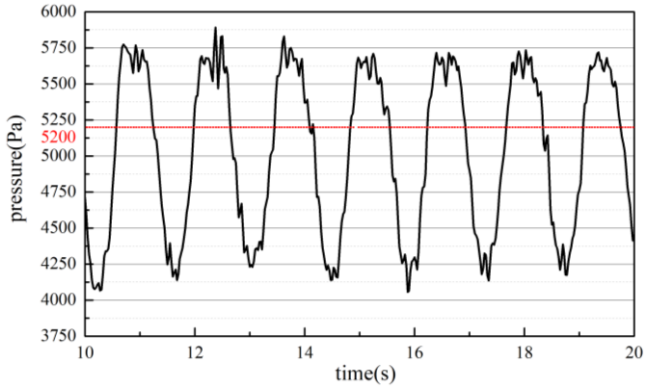

Fig.12 Pressure time curve at measuring point P3 for h_1=0.52m

Next, the motion of the cabin is analyzed. Fig.13 and Fig.14 show the sway motion of solid and liquid cabin under two filling rates respectively. For h_1=0.32m, as can be seen from Fig.13, the sway amplitude of liquid cabin is nearly the same as the solid cabin, only the motion phase of liquid cabin is earlier than that of solid cabin. This indicates that the liquid sloshing inside the cabin has little influence on the sway motion of the cabin. When the liquid filling rate is 75%, the sway motion amplitude of the liquid cabin is much smaller than that of the solid cabin, the liquid sloshing inside the cabin inhibits the sway motion of the cabin obviously. According to flow field at this filling rate shown in Fig.8, at the same time, the slamming pressure of the external regular wave on the cabin is in the opposite direction to that of the liquid inside the cabin, thus inhibiting the sway motion. However, when the filling rate of the cabin is 25%, it can be seen from Fig.3 that the fluid inside and outside the tank exerts the force on the same direction to the cabin, so the liquid sloshing inside the cabin further stimulates the sway motion of the cabin.

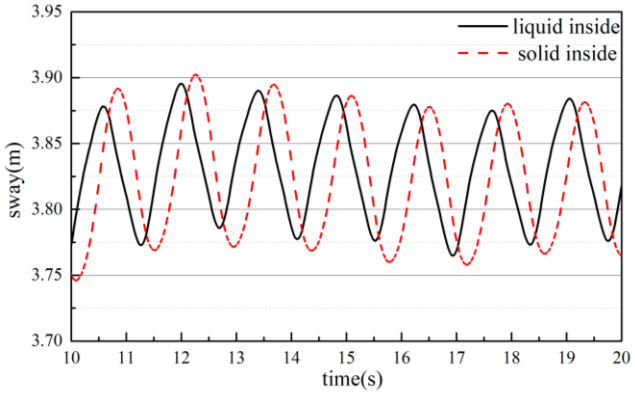

Fig.13 Comparison of sway motion between liquid cabin and solid cabin for h_1=0.32m

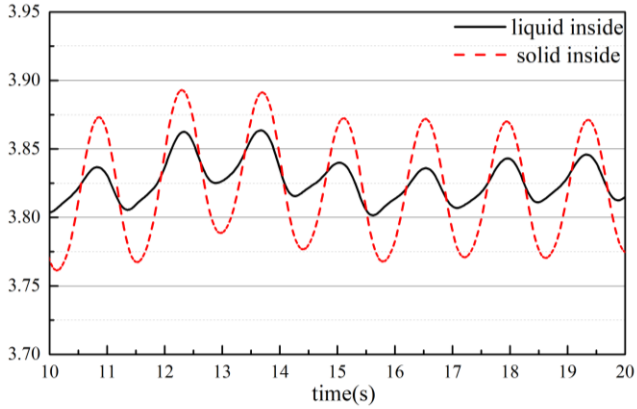

Fig.14 Comparison of sway motion between liquid cabin and solid cabin for h_1=0.52m

CONCLUSIONS

In this paper, the sway motion of a cabin with liquid inside in regular waves is simulated by in-house MPS solver, MLParticle-SJTU. The depth of liquid inside the cabin is changed, and the slamming pressure and the sway motion of the cabin are compared and analyzed. When the liquid filling rate is 50%, the sloshing phenomenon inside the cabin is the most intense. The meshless particle method used in this paper simulates the phenomenon of surface curling and wave breaking properly. There are two pressure peaks during each sway period, and the first pressure peak is higher than the second one. The liquid sloshing hits the front and the back bulkhead unevenly, the slamming pressure on the front bulkhead is higher than the back one, showing a slightly asymmetry. Whether the liquid sloshing inside the cabin promotes or inhibits the sway of the cabin is related to the depth of the liquid. For the cases simulated in this paper, the sway motion is promoted when the filling rate is 25%, the movement is inhibited when the filling rate is 75%. When the filling rate is 50%, the liquid sloshing

has little influence on the sway motion. The excitation or inhibition effect of the inside liquid sloshing on cabin movement depends on the phase difference between the liquid sloshing and the cabin sway motion, which is also related to the natural frequency of the liquid sloshing under different filling rate. The relationship among the filling rate, regular wave frequency and the sway motion will be further studied to find the conditions that will excite the resonance of the system.

ACKNOWLEDGEMENTS

This work was supported by the National Natural Science Foundation of China (52131102), and the National Key Research and Development Program of China (2019YFB1704200), to which the authors are most grateful.

REFERENCES

Cezar AB, Liang-YC, Tetsuo O, Makoto A (2019). "Optimized perforated bulkhead for sloshing mitigation and control," *Ocean Engineering*, 187, 106171.

Faltinsen, OM (1987). "A numerical nonlinear method of sloshing in tanks with two dimensional flow," *Journal of Ship Research*, 22(3), 193-202.

Felix-Gonzalez, I, Sanchez-Mondragon, J, Cruces-Giron, AR(2022). "Sloshing study on prismatic LNG tank for the vertical location of the rotational center," *Computational Particle Mechanics*, 9, 843–862.

Khayyer, A, Gotoh, H and Shao, S (2009). "Enhanced predictions of wave impact pressure by improved incompressible SPH methods," *Applied Ocean Research*, 31(2),111-131.

Lee, BH, Park, JC, Kim, MH, Hwang, SC (2011). "Step-by-step improvement of MPS method in simulating violent free-surface motions and impact-loads," *Computer Methods in Applied Mechanics and Engineering*, 200, 1113-1125.

Nakayama, T and Washizu, K (1980). "Nonlinear analysis of liquid motion in a container subjected to forced pitching oscillation," *International Journal for Numerical Methods in Engineering*, 15(8), 1207-1220.

Nakayama, T and Washizu, K (1981). "The boundary element method applied to the analysis of two-dimensional nonlinear sloshing problems," *International Journal for Numerical Methods in Engineering*, 17(11), 1631-1646.

Rueda, GE, Tsukamoto, MM, Medeiros, HF, et al (2008). "Validation study of MPS (moving particle semi-implicit method) for sloshing and damage stability analysis," *Proceedings of the ASME 2008 27th International Conference on Offshore Mechanics and Arctic Engineering*, Estoril, Portugal, ASME, 483-489.

Sanchez-Mondragon, J, Felix-Gonzalez, I, Cruces-Giron, AR (2022). "Turbulence analysis for vertical baffle configurations on prismatic tanks by the MPS method," *Ocean Engineering*, 264, 112392.

Tanaka, M and Masunaga, T (2010). "Stabilization and smoothing of pressure in MPS method by Quasi-Compressibility," *Journal of Computational Physics*, 229(11), 4279-4290.

Tsukamoto, MM, Cheng, LY, Nishimoto, K (2011). "Analytical and numerical study of the effects of an elastically-linked body on sloshing," *Computers & Fluids*, 49(1), 1-21.

Wen, X, Wan, DC (2018a). "Numerical simulation of three-layer-liquid sloshing by multiphase MPS method," *Proceedings of the ASME 2018 37th International Conference on Ocean, Offshore and Arctic Engineering*, Madrid, Spain, ASME, OMAE2018-78387.

Wen, X, Wan, DC, Chen, G (2018b). "Multiphase MPS method for two-layer liquid sloshing flows in oil-water separators" *Proceedings of the twenty-eighth (2018) International Ocean and Polar Engineering Conference*, Sapporo, Japan, ISOPE, 859-866.

Xue, MA and Lin, PZ (2011). "Numerical study of ring baffle effects on reducing violent liquid sloshing," *Computers & Fluids*, 52, 116-129.

Zhang, Y, Wan, D, Hino, T (2014). "Comparative study of MPS method and level-set method for sloshing flows," *Journal of Hydrodynamics*, 26(4), 577-585.

Zhang, YX, Wan, D, Hino, T (2014). "Application of MPS method in liquid sloshing," *The China Ocean Engineering*, 32(4), 24-32.

Zhang, YX, Wan, DC (2014). "Comparative study of MPS method and levelset method for sloshing flows," *Journal of Hydrodynamics*, 26(4), 577-585.

Zhang, YL, Chen, X, Wan, DC (2016). "MPS-FEM coupled method for the comparison study of liquid sloshing flows interacting with rigid and elastic baffles," *Applied Mathematics and Mechanics*, 37(12), 1359-1377.

Zhang, YL, Wan DC (2018). "MPS-FEM coupled method for sloshing flows in an elastic tank," *Ocean Engineering*, 152, 416-427.